INTERNATIONAL JOURNAL FOR NUMERICAL METHODS IN FLUIDS, VOL. 20, 1293–1314 (1995)

HOPF BIFURCATION IN ANNULAR LIQUID JETS WITH MASS TRANSFER

J. I. RAMOS

ETS Ingenieros Industriales, Universidad de Málaga, Plaza El Ejido, 29013 Málaga, Spain

SUMMARY

A numerical study of Hopf bifurcations in annular liquid jets with mass transfer is presented. The study is based on the asymptotic equations which govern the dynamics of inviscid, incompressible, thin, annular liquid jets and on equilibrium conditions for mass transfer at the jet's inner and outer interfaces. It is shown that the amplitude of the time-periodic motion that results from the Hopf bifurcation increases whereas its frequency decreases as the solubility ratio is increased.

KEY WORDS: chemical reactors; annular liquid jets; grid generation; mass absorption

1. INTRODUCTION

Annular liquid jets (Figure 1) may form enclosed volumes which can be used as chemical reactors for the reaction and control of toxic wastes, scrubbing of radioactive and non-radioactive materials, etc.[1] If annular liquid jets are used as chemical reactors, it is of paramount importance to determine the operating conditions (jet thickness, liquid mass flow rate at the nozzle exit, etc.) that maintain steady state operation and ensure that the gases generated by the combustion of toxic wastes in the volume enclosed by the annular jet are absorbed by the liquid and do not leak through the jet's outer interface. Unfortunately, the binary diffusion coefficients of gases in liquids are small and as a consequence the amount of gases absorbed by the liquid is small.[2,3] On the other hand, since the thermal conductivity of liquids is in general larger than that of gases, the liquid jet absorbs heat at a much faster rate than it absorbs the gases generated in the combustion of toxic wastes. This implies that heat transfer phenomena are much faster than mass absorption and may be considered as instantaneous on the time scale of mass transfer.

Since the mass absorption rate by the liquid is small, the gases generated in the combustion of toxic products may accumulate within the volume enclosed by the annular jet, thus increasing the pressure of these gases. However, the pressure build-up within the volume enclosed by the jet cannot exceed a critical value beyond which the jet becomes unstable and/or does not form an enclosed volume.

Analytical and asymptotic studies of thin, inviscid, incompressible, annular liquid jets[4,5] have shown that for a nozzle exit angle of 0° the jet exhibits a cylindrical geometry for a pressure coefficient equal to unity. These analytical and numerical studies have also shown that the convergence length of the annular liquid jet, defined as the axial location at which the inner radius is zero, increases as the pressure of the gases enclosed by the annular jet exceeds that of the gases surrounding the jet. Furthermore, as the convergence length increases, it is expected that small perturbations may cause Kelvin–Helmholtz and/or Rayleigh–Taylor instabilities that may break the jet up with the consequent

CCC 0271–2091/95/121293–22

Received 28 August 1992
Revised 31 August 1993

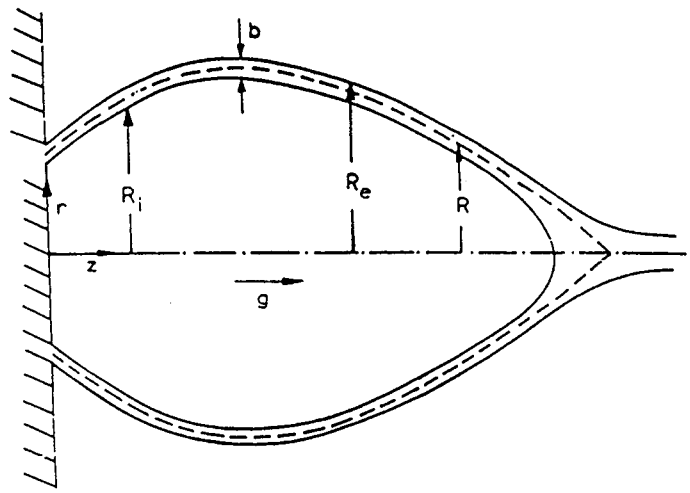

Figure 1. Schematic of an annular liquid jet

formation of ligaments and droplets. For these reasons it is convenient to investigate the effects that the non-dimensional parameters that govern the dynamics of and mass absorption by annular liquid jets have on the annular jet stability. Unfortunately, the fluid dynamics of inviscid, incompressible, annular liquid jets depends on the Froude and Weber numbers, the jet angle and thickness at the nozzle exit, the initial pressure of the gases enclosed by the jet and a pressure coefficient which is a function of the pressure exerted by the gases surrounding the liquid jet and the surface tension. If the friction of the gases surrounding the liquid is also considered, the Reynolds number based on the density and dynamic viscosity of these gases must also be considered.[6] Fortunately, friction effects on the fluid dynamics of steady state jets are not important except at low Reynolds numbers and/or large positive angles at the nozzle exit.[6].

For low-Mach-number flows the pressure within the volume enclosed by the annular liquid jet is nearly homogeneous and, since the mass and thermal diffusivities of gases are larger than those of liquids, both the temperature and concentration of the gases enclosed by the annular jet may be assumed uniform as a first approximation, even though these gases are entrained by the liquid's inner interface and may form toroidal recirculation zones. If these assumptions are made and the gas–liquid interfaces are assumed to be in equilibrium, then the isothermal mass transfer between the liquid and the gases enclosed by the annular jet depends on the mass Peclet number, the ratio of the solubilities at the inner and outer interfaces of the annular jet, the concentration of the gases dissolved in the liquid at the nozzle exit and the temperature. Therefore, the dynamics of and mass absorption by inviscid, incompressible, isothermal, annular liquid jets depends on 10 parameters, space and time. The high dimensionality of the parameter space does not permit one to investigate the possibly rich dynamics of annular liquid jets. For this reason, most studies have focused on analysing the mass absorption under steady state conditions. For example, Baird and Davidson[7] studied mass absorption by steady annular liquid jets using the von Mises transformation and obtained analytical solutions for nearly vertical jets in zero gravity. Ramos and Pitchumani[8] used the von Mises transformation and Lagrangian co-ordinates, whereas Ramos[9,10] employed Eulerian co-ordinates and the von Mises transformation[9] and a linear mapping,[10] to determine the steady state mass absorption rate.

The analytical and numerical studies presented in References 9 and 10 are based on the asymptotic fluid dynamics equations derived by Ramos[5] for thin, annular liquid jets. These asymptotic equations

can be obtained by integrating the Navier–Stokes equations across the annular jet thickness, expanding the flow variables along the annular jet mean radius, applying kinematic conditions at the annular jet mean radius, neglecting both axial pressure variations in the liquid and friction effects on the inner and outer interfaces of the annular liquid jet and assuming inviscid liquids. By way of contrast, the analytical and numerical results reported by Ramos and Pitchumani[8] are based on the equations derived by Ramos[4] along and normal to the annular liquid-jet interfaces and assume that the velocity is uniform across the annular jet thickness. As shown in Reference 5, the fluid dynamics equations employed by Baird and Davidson[7] and Ramos and Pitchumani[8] correspond to the leading term of the asymptotic equations derived in Reference 5. All these studies are based on the assumption that the gas–liquid interfaces are clean and that mass transfer resistances are small;[2,3] therefore, all of them assumed equilibrium interfaces.

The analytical studies of Baird and Davidson,[7] Ramos and Pitchumani[8] and Ramos[9,10] were based on the assumption that, in order to maintain steady operating conditions, mass had to be injected into the volume enclosed by the annular jet at a rate equal to the mass absorption rate by the liquid. If the mass injection rate is larger than the mass absorption rate, the volume enclosed by the liquid will increase with time. On the other hand, if the mass absorption rate by the liquid is larger than the mass injection rate into the volume enclosed by the annular liquid jet, this will collapse. Numerical studies of jet collapse due to mass absorption have also been reported.[11,12]

In both steady state and time-dependent studies of mass absorption by annular liquid jets, the effect of each parameter on mass absorption was examined while keeping the remaining parameters fixed. This corresponds to a one-dimensional exploration of the 10-dimensional parameter space. These studies, however, indicated that qualitative changes in the dynamics of and mass absorption by annular liquid jets were possible, although they were not investigated.

In order to increase the mass transfer rates between the liquid and the gases generated in the combustion of toxic products within the volume enclosed by the annular liquid jet, one many consider overpressurized jets, large Weber numbers, etc., which result in long jets and large surface areas available for mass transfer.[9,10]. Unfortunately, long jets may become unstable and break up. Therefore other means to increase the mass transfer rates between the liquid and gases must be investigated. A technique which may yield enhanced mass transfer is to use pulsating or oscillatory liquid mass flow rates at the nozzle exit. These oscillations may cause modulations and compression and expansion of the gases enclosed by the annular liquid jet. If the mass enhancement during the compression part of the oscillations is larger than the decrease in mass transfer during the expansion part of the oscillations, a phenomenon known as mass rectification results. Unfortunately, the control of both the oscillatory mass flow rate at the nozzle exit and the dynamics of annular liquid jets demands that special techniques be designed in order to maintain stable, yet oscillating, operating conditions. However, a different means to enhance gas–liquid mass transfer can be achieved by considering the physics of mass absorption and its dependence on the non-dimensional parameters that control it. For example, mass absorption by annular liquid jets is a highly non-linear phenomenon that depends in an integrodifferential, non-linear manner on the mass of the gases enclosed by the annular jet, and this mass affects both the gas concentration and the pressure at the inner interface.[9,12] It is therefore possible that by varying the non-dimensional parameters that most affects the pressure of the gases enclosed by the annular jet, enhanced mass transfer may be achieved.

The results presented in this paper were found when exploring the effects of the ratio of the gas solubilities at the gas–liquid inner and outer interfaces on the annular liquid jets dynamics and correspond to underpressurized, annular liquid jets when the combustion of toxic wastes taking place under steady, isothermal conditions in the volume enclosed by the jet is extinguished. In most cases, physical intuition indicates that, once there is no generation of gases in the volume enclosed by the

annular jet, this should collapse owing to mass transfer to the liquid. The results presented in this paper indicate that this is so for certain solubilities and that there is a solubility ratio at which the fluid dynamics and mass transfer phenomena in annular liquid jets exhibit a Hopf bifurcation that results in enhanced mass transfer.

Since the derivation of the equations governing the fluid dynamics of and mass transfer by thin, annular jets and the numerical method used to solve the governing equations have been presented in great detail elsewhere,[9,12] only a brief summary of these equations is presented in the following sections.

2. GOVERNING EQUATIONS

The asymptotic equations that govern the fluid dynamics of axisymmetric, thin, inviscid incompressible, annular liquid jets can be obtained by averaging the Navier–Stokes equations across the annular jet and including the kinematic and stress conditions at the jet's inner and outer inferfaces which are material surfaces. At each gas–liquid interface the shear stress is continuous whereas the jump in normal stresses is balanced by surface tension.[5] These equations have been derived in detail in Reference 5 and only a summary of them is presented in the next subsection.

2.1. *Fluid dynamics equations*

The non-dimensional, asymptotic equations which govern the fluid dynamics of thin, inviscid, annular liquid jets are[5]

$$\mathbf{U}_t + \mathbf{F}_z = \mathbf{G}, \tag{1}$$

where

$$\mathbf{U} = [m,\ mR,\ mu,\ m\bar{v}]^{\mathrm{T}}, \qquad \mathbf{F} = [mu,\ mRu,\ muu,\ mu\bar{v}]^{\mathrm{T}}, \tag{2}$$

$$\mathbf{G} = \left[0,\ m\bar{v},\ \frac{m}{Fr} + \frac{1}{We}\left(\frac{\partial J}{\partial z} - C_{\mathrm{pn}}R\frac{\partial R}{\partial z}\right),\ \frac{1}{We}\left(C_{\mathrm{pn}}R - \frac{\partial J/\partial z}{\partial R/\partial z}\right)\right]^{\mathrm{T}}, \tag{3}$$

$$\mathbf{U}(t,\ 0) = [1,\ 1,\ 1,\ \tan\ \theta_0]^{\mathrm{T}}, \tag{4}$$

$$J = R\Big/\left[1 + \left(\frac{\partial R}{\partial z}\right)^2\right]^{1/2}, \tag{5}$$

$$R_{\mathrm{e}} = R + b/2, \qquad R_{\mathrm{i}} = R - b/2, \tag{6}$$

$$b = R_{\mathrm{e}} - R_{\mathrm{i}}, \qquad R = (R_{\mathrm{e}} + R_{\mathrm{i}})/2, \qquad b = (m/R)(b_0^*/R_0^*), \tag{7}$$

$$Fr = u_0^{*2}/gR_0^*, \qquad We = m_0^* u_0^{*2}/2\sigma R_0^*, \tag{8}$$

$$C_{\mathrm{pn}} = C_{\mathrm{p}}We, \qquad C_{\mathrm{p}} = (p_{\mathrm{i}}^* - p_{\mathrm{e}}^*)R_0^{*2}/m_0^* u_0^{*2}, \tag{9}$$

the superscript 'T' denotes transpose, Fr and We are the Froude and Weber numbers respectively, m is the annular liquid jet mass per unit length, u and $\bar{v}$ are the mean axial and radial velocity components of the liquid respectively, p is the pressure, R and b are the jet mean radius and thickness respectively, t is time, z is the axial co-ordinate, C_{pn} denotes the pressure coefficient, the

asterisk denotes dimensional quantities, θ_0 is the nozzle exit angle, i.e. the angle at which the liquid leaves the nozzle, and the subscripts 'i', 'e' and '0' denote the inner and outer interfaces and the nozzle exit respectively.

In the above equations, length, time, velocity components and mass per unit length have been non-dimensionalized with respect to R_0^*, R_0^*/u_0^*, u_0^*, and $m_0^*=\rho R_0^* b_0^*$ respectively, where ρ is the liquid density. The initial conditions required for the solution of equations (1)–(4) correspond to the solution of these equations when the combustion of toxic wastes generates gaseous products at a rate equal to the mass absorption rate by the liquid. Under these conditions, the fluid dynamics of and the mass absorption by annular liquid jets are uncoupled. Once the combustion of toxic wastes is extinguished, the gases in the volume are absorbed by the liquid and the dynamics of the latter is coupled to the mass transfer phenomena. Time $t = 0$ corresponds to the time at which combustion is extinguished.

The pressure coefficient (see equation (9)) can be written as

$$C_{\mathrm{pn}} = C_{\mathrm{pmax}}\left(\frac{p_{\mathrm{i}}^*}{p_{\mathrm{e}}^*} - 1\right), \tag{10}$$

where

$$C_{\mathrm{pmax}} = p_{\mathrm{e}}^* R_0^*/2\sigma \tag{11}$$

and σ denotes the surface tension.

The convergence length can be obtained from the condition that at the convergence point the inner radius of the annular liquid jet is zero, i.e. (see equation (6))

$$R_i(t, z = L(t)) = 0, b(t, z = L(t)) = 2R(t, z = L(t)), \tag{12}$$

which implies that (see equation (7))

$$2R^2(t, z = L(t)) = b_0^* \frac{m(t, z = L(t))}{R_0^*}. \tag{13}$$

Differentiation of equation (13) with respect to t yields

$$4R\frac{\mathrm{d}R}{\mathrm{d}t} = 4R\left(\frac{\partial R}{\partial t} + \frac{\partial R}{\partial z}\frac{\mathrm{d}L}{\mathrm{d}t}\right) = \frac{b_0^*}{R_0^*}\left(\frac{\partial m}{\partial t} + \frac{\partial m}{\partial z}\frac{\mathrm{d}L}{\mathrm{d}t}\right) \quad \text{at } z = L(t). \tag{14}$$

Use of equation (1) in equation (14) implies that

$$4R\left(\bar{v} - u\frac{\partial R}{\partial z} + \frac{\partial R}{\partial z}\frac{\mathrm{d}L}{\mathrm{d}t}\right) = \frac{b_0^*}{R_0^*}\left(-\frac{\partial (mu)}{\partial z} + \frac{\partial m}{\partial z}\frac{\mathrm{d}L}{\mathrm{d}t}\right) \quad \text{at } z = L(t), \tag{15}$$

which is an ordinary differential equation for the convergence length.

2.2. *Gases enclosed by the liquid*

Since the mass diffusivities of gases are much higher than the binary diffusion coefficients of gases in liquids, it may be assumed that the concentration of the gases enclosed by the liquid is uniform. If, in addition, these gases are assumed to be ideal and isothermal at the temperature T_i^* and consists of a single species and the Mach number is small, the pressure of the gases enclosed by the annular liquid jet can be assumed to be uniform and can be determined as[9,10]

$$p_{\mathrm{i}}^* = \frac{M_{\mathrm{i}}^* \tilde{R} T_{\mathrm{i}}^*}{\pi R_0^{*3}}\left(m_{\mathrm{i}} \Big/ \int_0^L R_{\mathrm{i}}^2 \,\mathrm{d}z\right), \qquad \frac{p_{\mathrm{i}}^*}{p_{\mathrm{e}}^*} = \frac{m_{\mathrm{i}}}{V}, \tag{16}$$

where

$$m_i = m_i^*/M_i^*, \qquad M_i^* = \pi R_0^{*3} p_e^*/\tilde{R}T_i^*, \qquad V = \int_0^L R_i^2 \, dz, \tag{17}$$

$\tilde{R}$ is the specific gas constant, L is the non-dimensional convergence length, i.e. the axial distance measured from the nozzle exit at which the inner radius of the annular liquid jet becomes zero, and V is the non-dimensional volume of the gases enclosed by the annular liquid jet.

The gases surrounding the liquid jet are assumed to be ideal, isothermal, single-component, identical to those enclosed by the jet and infinite in extent, so that p_e^* can be assumed to be constant.

Substitution of equation (16) and (17) into equation (10) yields

$$C_{pn} = C_{p\max}\left(m_i \Big/ \int_0^L R_i^2 \, dz - 1\right). \tag{18}$$

It is clear from equation (1) and (18) that the fluid dynamics of annular liquid jets depends on m_i, which in turn depends on the mass absorbed by the liquid and on the mass injected into and/or the mass generated by the combustion of toxic products in the volume enclosed by the jet. In the absence of mass injection or mass generation, m_i depends on the mass absorbed by the liquid as determined in the followng subsections.

2.3. *Gas concentration in the annular liquid jet*

If volumetric displacement effects due to the gas absorved by the liquid are small, the liquid may be assumed to be incompressible and the gas concentration in the liquid is governed by the non-dimensional equations[9–12]

$$\frac{\partial u}{\partial z} + \frac{1}{r}\frac{\partial}{\partial r}(rv) = 0, \tag{19}$$

$$\frac{\partial c}{\partial t} + u\frac{\partial c}{\partial z} + v\frac{\partial c}{\partial r} = \frac{1}{Pe}\left[\frac{1}{r}\frac{\partial}{\partial r}\left(r\frac{\partial c}{\partial r}\right) + \frac{\partial^2 c}{\partial z^2}\right], \tag{20}$$

$$c(t, r, 0) = \alpha(\beta - 1), \quad R_i(t, 0) < r < R_e(t, 0), \tag{21}$$

$$c(t, R_i(t, z), z) = \alpha\left(\gamma \frac{m_i}{\int_0^L R_i^2 \, dz} - 1\right), \tag{22}$$

$$c(t, R_e(t, z), z) = 0, \tag{23}$$

$$u\frac{\partial c}{\partial z} + v\frac{\partial c}{\partial r} = 0, \quad \text{at } z = L(t), \tag{24}$$

$$Pe = u_0^* R_0^*/D^*, \qquad \alpha = 2\tilde{R}T_i^* S_e, \qquad \beta = c_0^*/S_e p_e^*, \qquad \gamma = S_i/S_e = H_e/H_i, \tag{25}$$

where Pe is the Peclet number, $S_i = H_i^{-1}$ and $S_e = H_e^{-1}$ denote the solubilities at the annular jet's inner and outer surfaces respectively, H_i and H_e denote the Henry constants at the annular jet's inner and outer interfaces respectively, D^* is the diffusivity of the gas in the liquid and c_0^* is the dimensional gas concentration at the nozzle exit.

2.4. Mass absorption by the annular liquid jet

The non-dimensional mass transfer rate at the inner and outer interfaces can be written as[9–12]

$$\frac{dm_i}{dt} = \frac{1}{Pe} \int_0^L R_i \frac{\partial c}{\partial r}(t,\ R_i(t,\ z),\ z)\,(1 + \tan^2\ \theta_i)\ dz \tag{26}$$

subject to

$$m_i(0) = \frac{p_i^*(0)}{p_e^*} \int_0^L R_i^2(0,\ z)\ dz, \tag{27}$$

where equation (16) has been used and

$$\tan\ \theta_i = \frac{\partial R_i}{\partial z} \tag{28}$$

The non-dimensional mass flux at the outer surface of the annular jet can be determined by analogy with equation (26) as

$$\frac{dm_e}{dt} = -\frac{1}{Pe} \int_0^L R_e \frac{\partial c}{\partial r}(t,\ R_e(t,\ z),\ z)\,(1 + \tan^2\ \theta_e)\ dz, \tag{29}$$

where

$$\tan\ \theta_e = \frac{\partial R_e}{\partial z} \tag{30}$$

Equations (1), (19)–(24), (26) and (27) indicate that in the absence of both mass injection and mass generation by the combustion of toxic products in the volume enclosed by the annular liquid jet, its dynamics depends on $b_0^*/R_0^*, C_{pmax}, Pe, \alpha, \beta, \gamma, Fr, We, \theta_0$ and $p_i^*(0)/p_e^*$.

Equations (1), (19), (20) and (26) represent a system of integrodifferential equations. In order to solve these equations, it is required to first evaluate v, i.e. the local radial velocity, which can be calculated by integrating equation (19) from $R_i(t,z($ to r to obtain

$$vr = v(t,\ R_i,\ z)R_i(t,\ z) - \frac{\partial}{\partial z}\left(u\,\frac{r^2 - R_i^2}{2}\right) - uR_i\,\frac{\partial R_i}{\partial z}, \tag{31}$$

where Leibnitz's rule has been used and u has been assumed to be only a function of t and z. This assumption can be justified, since the gases surrounding and enclosed by the jet have much smaller dynamic viscosities than the liquid and therefore cannot introduce strong velocity variations across the annular jet. This assumption is not valid near the nozzle exit, where the liquid relaxes from stick boundary conditions at the nozzle walls to slip/free boundary conditions at the jet interfaces.[5] It is also not valid near the convergence point, i.e. near $z = L$, where a meniscus and an axial pressure gradient exist. Axial and radial pressure gradients were neglected in the derivation of equation (1).[5]

Since the inner and outer surfaces of the annular jet are material surfaces,

$$v(t,\ R_i,\ z) = \frac{\partial R_i}{\partial t} + u\,\frac{\partial R_i}{\partial z}, \tag{32}$$

$$v(t,\ R_e,\ z) = \frac{\partial R_e}{\partial t} + u\,\frac{\partial R_e}{\partial z}. \tag{33}$$

Substitution of equation (32) into equation (31) yiields

$$vr = R_i \frac{\partial R_i}{\partial t} - \frac{\partial}{\partial z}\left(u \frac{r^2 - R_i^2}{2}\right) \tag{34}$$

and the value of $R_i (= R - b/2)$ can be calculated from equation (6).

3. NUMERICAL METHODS

The annular liquid jet geometry is curvilinear and time-dependent and has an unknown, time-dependent, downstream boundary. This geometry can be transformed into a unit square by means of the mapping[10–12]

$$(t, r, z) \rightarrow (\tau, \xi, \eta), \tag{35}$$

where

$$\tau = t, \qquad \xi = (r - R_i)/b, \qquad \eta = z/L, \tag{36}$$

with $R_i = R_i(t, z), b = b(t, z) = R_e - R_i$ and $L = L(t)$.

The Jacobian of this mapping is

$$\mathbf{J} = \frac{\partial(t, r, z)}{\partial(\tau, \xi, \eta)} = bL \tag{37}$$

and is therefore a function of z and t.

3.1. Fluid dynamics equations

Substitution of equations (36) and (37) into equation (1) yields

$$\mathbf{V}_\tau + (\mathbf{V}\bar{\mathbf{u}})_\eta = L\mathbf{G}, \tag{38}$$

where

$$\mathbf{V} = \mathbf{U}L. \tag{39}$$

A conservative, finite volume technique was used to discretize equation (38) on a staggered grid, where the convective terms were discretized by means of upwind or donor cell differences. The value of $\mathbf{V}$ at the convergence point, i.e. at η=1, was determined from linear extrapolation. Upwind differences were also used to discretize the spatial derivatives which appear in the ordinary differential equation for L (see equation (15)). The resulting system of coupled, algebraic, non-linear equations for $\mathbf{V}$ and L was solved iteratively until

$$\left(\sum_{i=2}^{NI} \Delta\mathbf{W}_i^{\mathrm{T}} \cdot \Delta\mathbf{W}_i\right)^{1/2} \leq \varepsilon_1, \tag{40}$$

where

$$\mathbf{W} = (\mathbf{V}_2^{\mathrm{T}}, \mathbf{V}_3^{\mathrm{T}}, \ldots, \mathbf{V}_{NI}^{\mathrm{T}}, L)^{\mathrm{T}}, \qquad \Delta\mathbf{W} = \mathbf{W}^{k+1} - \mathbf{W}^k, \tag{41}$$

NI is the number of grid points used in the calculations, k denotes the kth iteration within the time step and $\epsilon_1 = 10^{-6}$.

3.2. *Gas concentration equation*

Introducing the mapping defined by equation (36) and (37) into the gas concentration equation (see equation (20)) yields

$$(r\mathbf{J}c)_\tau + (r\mathbf{J}c\bar{\bar{v}})_\xi + (r\mathbf{J}c\bar{u})_\eta = Pe^{-1}\left[\left(r\frac{L}{b}c_\xi\right)_\xi + \left[\xi_z(\mathbf{J}\xi_z c)_\xi + \xi_z(\mathbf{J}c\eta_z)_\eta\right]_\xi + \left[\eta_z(\mathbf{J}\xi_z c)_\xi + \eta_z(\mathbf{J}\eta_z c)_\eta\right]_\eta\right], \tag{42}$$

where

$$\bar{\bar{v}} = \xi_t + u\xi_z + v\xi_r, \tag{43}$$

$$c(\tau,\ 0,\ \eta) = \alpha\left(\frac{\gamma m_i}{L\int_0^1 R_i^2\,\mathrm{d}\eta} - 1\right), \tag{44}$$

$$c(\tau,\ 1,\ \eta) = 0, \tag{45}$$

$$c(\tau,\ \xi,\ 0) = \alpha(\beta - 1), \tag{46}$$

$$(\mathbf{J}crv^*)_\xi + (\mathbf{J}cru^*)_\eta = 0 \quad \text{at } (\tau,\ \xi,\ 1), \tag{47}$$

$$v^* = u\xi_z + v\xi_r, \qquad u^* = u\eta_z. \tag{48}$$

A conservative, finite volume technique on a staggered grid with upwind or donor cell treatment of the convection terms was employed to discretize equation (42) and (47) and the resulting system of algebraic equations was solved iteratively by means of a line Gauss–Seidel method that swept the computational domain from the nozzle exit to the convergence point as many times as required until the following convergence criterion was satisfied:

$$\sum_{i=2}^{NI}\sum_{j=2}^{NJ}(\Delta c_{i,j}^k)^2 \le \varepsilon_2, \tag{49}$$

where $\Delta c^k = c^{k+1} - c^k, NJ$ is the number of grids points in the radial direction and $\varepsilon_2 = 10^{-6}$. Therefore, at each axial location a tridiagonal system of algebraic equations was solved.

3.3. *Mass absorption rate*

In order to obtain accurate results and to avoid the mathematical incompatibilities that may exist at the nozzle exit,[9,10] the following rectangular rule was used to calculate the mass absorption rate at the jet's inner interface:

$$\frac{\mathrm{d}m_i}{\mathrm{d}\tau} = \frac{L}{Pe}\sum_{k=2}^{NI-1}\left(\frac{R_i}{b}\right)_k \frac{c_{k,2} - c_{k,3/2}}{\Delta\xi/2}(1 + \tan^2\theta_i)_k\Delta\eta, \tag{50}$$

which does not involve the value of $\partial c/\partial\xi$ at (ξ,η)=(0,0).

Since the pressure of the gases enclosed by the annular liquid jet affects the fluid dynamics and gas concentration equations (see equation (3), (9), (10), (18) and (22)), in addition to the convergence

criteria defined by equation (40) and (49), the following criteria were also used in the calculations presented in this paper:

$$\varepsilon_{\text{abs}} = \left| \left(\frac{\mathrm{d}m_{\text{i}}}{\mathrm{d}\tau} \right)^{k+1} - \left(\frac{\mathrm{d}m_{\text{i}}}{\mathrm{d}\tau} \right)^{k} \right| \leq \varepsilon_3, \tag{51}$$

$$\varepsilon_{\text{rel}} = \varepsilon_{\text{abs}} \Bigg/ \left| \left(\frac{\mathrm{d}m_{\text{i}}}{\mathrm{d}\tau} \right)^{k+1} \right| \leq \varepsilon_4, \tag{52}$$

where ε_3 and ε_4 are user-specific error tolerances.

The relative error defined in equation (52) was used because the mass absorption rate is small and decreases as the Peclet number is increased.

The convergence criteria defined by equation (40), (49), (51) and (52) are a bit redundant, since m_i affects $\mathbf{V}, L$ and c, and only one of them may be necessary.

In the calculations presented in this paper, $\varepsilon_3 = \varepsilon_4 = 10^{-7}$.

3.4. *Initialization*

The formulation presented in this paper can be used to study both steady state and time-dependent problems. Under steady state conditions, mass is injected into or generated by the combustion of toxic wastes in the volume enclosed by the annular jet at a rate equal to the mass absorption rate by the liquid, p_{i}^* and m_{i} are constant, the boundary conditions are independent of time, $\mathrm{d}L/\mathrm{d}\tau = 0$ and the fluid dynamics and gas concentration equations are not coupled.

The asymptotic steady state obtained from the solution of the equations presented in this paper subject to time-independent boundary conditions is achieved when the following criteria are satisfied:

$$\left(\sum_{i=2}^{NI} \frac{\Delta \mathbf{W}_i^{\text{T}} \cdot \Delta \mathbf{W}_i}{\Delta \tau^2} \right)^{1/2} \leq \varepsilon_5, \tag{53}$$

$$\sum_{i=2}^{NI} \sum_{j=2}^{NJ} (\Delta c_{i,j})^2 \leq \varepsilon_6, \tag{54}$$

$$\varepsilon_{\text{abs}} = \left| \Delta \left(\frac{\mathrm{d}m_{\text{i}}}{\mathrm{d}\tau} \right) \right| \leq \varepsilon_7, \qquad \varepsilon_{\text{rel}} = \varepsilon_{\text{abs}} \Bigg/ \left| \left(\frac{\mathrm{d}m_{\text{i}}}{\mathrm{d}\tau} \right)^{n+1} \right| \leq \varepsilon_8, \tag{55}$$

where, for example,

$$\Delta \mathbf{W} = \mathbf{W}^{n+1} - \mathbf{W}^{n}, \tag{56}$$

the superscript n denotes the nth time step, $\varepsilon_5 = \varepsilon_6 = 10^{-6}$ and $\varepsilon_7 = \varepsilon_8 = 10^{-7}$.

Once steady state was achieved, τ was set to zero and $(m_i)_{\text{ss}} = m_{\text{i}}(0)$ and $(p_{\text{i}}^*)_{\text{ss}} = p_{\text{i}}^*(0)$, where 'ss' denotes steady state, were calculated. These initial conditions were then used to analyse the jet dynamics in the absence of mass injection into or mass generation by the combustion of toxic products in the volume enclosed by the annular liquid jet. Note that in the absence of mass injection and mass generation, the mass of the gas enclosed by the annular liquid jet is governed by the equation

$$m_{\text{i}}(\tau) = m_{\text{i}}(0) + \int_0^{\tau} \frac{\mathrm{d}m_{\text{i}}}{\mathrm{d}t} \, \mathrm{d}t, \tag{57}$$

which can be discretized as

$$m_i^{n+1} = m_i^n + \Delta\tau\left(\frac{dm_i}{d\tau}\right)^{n+1} \tag{58}$$

subject to $m_i^0 = m_i(0)$.

4. PRESENTATION OF RESULTS

As shown in Section 2, the fluid dynamics of and mass absorption by annular liquid jets depend on several dimensionless parameters. The values of the parameters used in this paper are $Pe = 10^6$, $Fr = 10, We = 25, b_0^*/R_0^* = 0{\cdot}05, \theta_0 = 0, \alpha = 1, \beta = 1, C_{pmax} = 1$ and $p_i^*(0)/p_e^* = 0{\cdot}75$. The value of γ was varied as indicated in the next paragraphs. The convergence length corresponding to these parameters at time $t = 0$, i.e. the rate of generation of gaseous combustion products is equal to the mass absorption rate by the liquid, is $L(0) = 4{\cdot}28$.

All the calculations presented in this paper were performed in double-precision arithmetic and the time and spatial step sizes were varied so as to ensure that the calculations were grid-independent. It was observed that if the grid spacings in the axial and radial directions and the time step were not small enough, the mass transfer rates were inaccurately calculated and this resulted in inaccurate dynamics and poor resolution of the steep flow gradients in the gas concentration at the annular liquid jet's inner interface, pressure coefficients and mass transfer rates. The largest values of the time step and grid spacings in the axial and radial directions were 0·001, 0·01 and 0·0005 respectively.

Figure 2 shows the pressure coefficient, the convergence length normalized by its initial value and the thickness and mean radius of the annular liquid jet at the convergence point for $\gamma = 2$. These quantities are monotonic functions of time and tend to asymptotic equilibrium, steady state values which correspond to a gas concentration at the inner interface equal to that at the outer interface, i.e. zero concentration at both interfaces and zero mass transfer rates. Although not shown here, both the liquid axial velocity at the convergence point and the volume of the gases enclosed by the annular jet decrease monotonically as functions of time until a steady state is reached.

Figure 2 also indicates that the convergence length which has been normalized by its initial value

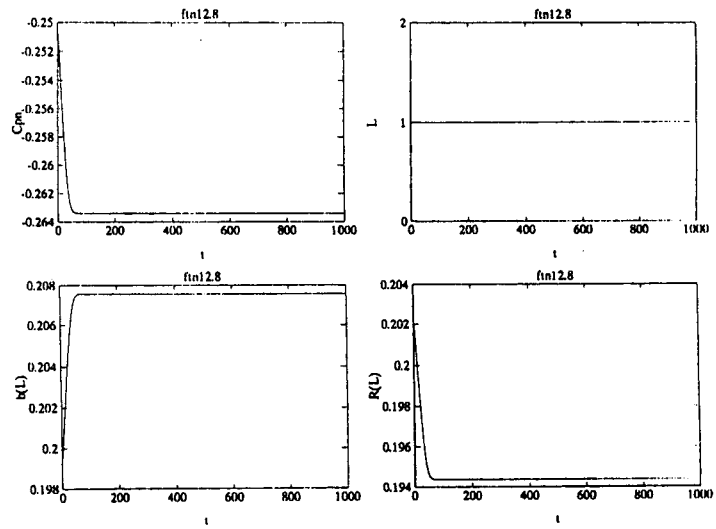

Figure 2. Pressure coefficient, convergence length and annular jet thickness and mean radius at the convergence point as functions of time for γ=2

does not change with time. This result is consistent with the analytical and numerical solutions of steady state, annular jets[4,5] which show that the convergence length is a weak function of the initial pressure of the gases enclosed by the jet.

Figure 3 shows the phase diagrams for the convergence length and jet thickness and mean radius at the convergence point and indicates that both the initial and final states are fixed equilibrium points. Figure 4 shows that the mass transfer rates at both the inner and outer interfaces increase with time until a steady state corresponding to mass transfer rates equal to zero is reached. The mass of the gases enclosed by the jet decreases monotonically with time; the steady state mass of the gases enclosed by the annular jet is approximately equal to 97·75% of the initial mass. Although not shown here, the volume of the gases enclosed by the annular jet also decreases as a function of time and its asymptotic steady state value is approximately 99·45% of its initial value.

Figures 5–7 indicate that for γ=4 the pressure coefficient and jet thickness and mean radius at the convergence point converge oscillatorily towards an equilibrium steady state. These oscillations are indicative that a topological change is about to occur as illustrated in the phase diagrams shown in Figure 6, which indicate that the solution approaches the equilibrium state spirally. The mass transfer rates at the inner and outer interfaces and the mass of the gases enclosed by the annular liquid jet also exhibit damped oscillations (see Figure 7).

The oscillatory behaviour observed in Figures 5–7 was also seen for values of γ less than or equal to 4·8; however, the time required for these oscillations to be damped out increased as γ was increased as illustrated in Figures 8–10, which correspond to γ = 4·8. These figures show that small oscillations in the pressure coefficient, jet thickness and mean radius at the convergence point, mass transfer rates at the inner and outer interfaces and mass of the gases enclosed by the annular jet are still present at t = 1000. The phase diagrams shown in Figure 9 also indicate the spiral convergence of both the thickness and mean radius of the annular liquid jet at the convergence point towards their equilibrium steady states.

For a value of γ = 4·9 the results presented in Figures 11–13 indicate that the pressure coefficient is a periodic function of time which has an amplitude approximately equal to 0·00026. This is clearly indicated in the phase diagrams presented in Figure 12, which show that the amplitudes of both the

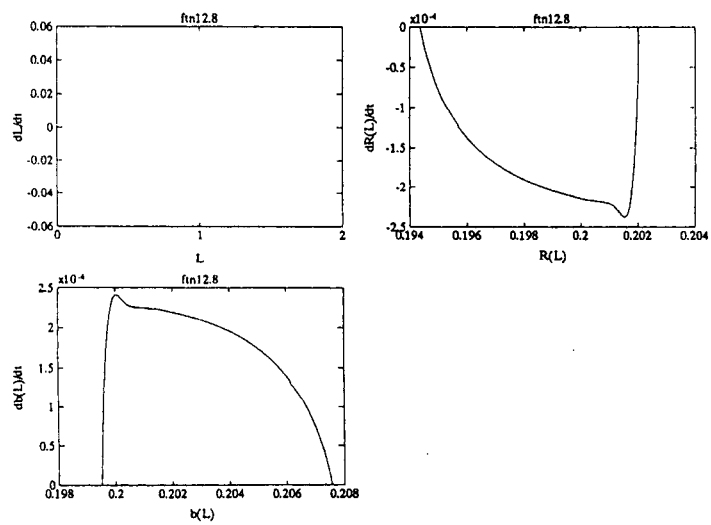

Figure 3. Phase diagrams for γ=2

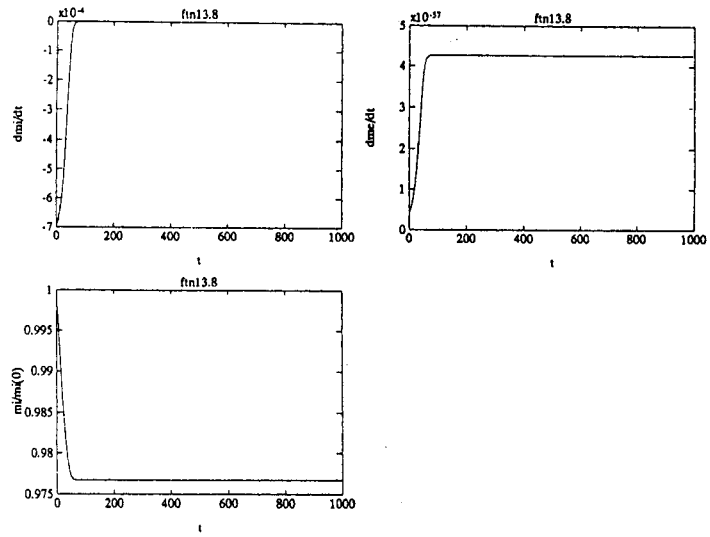

Figure 4. Mass transfer rates at the inner and outer interfaces and mass of the gases enclosed by the annular jet as functions of time for γ=2

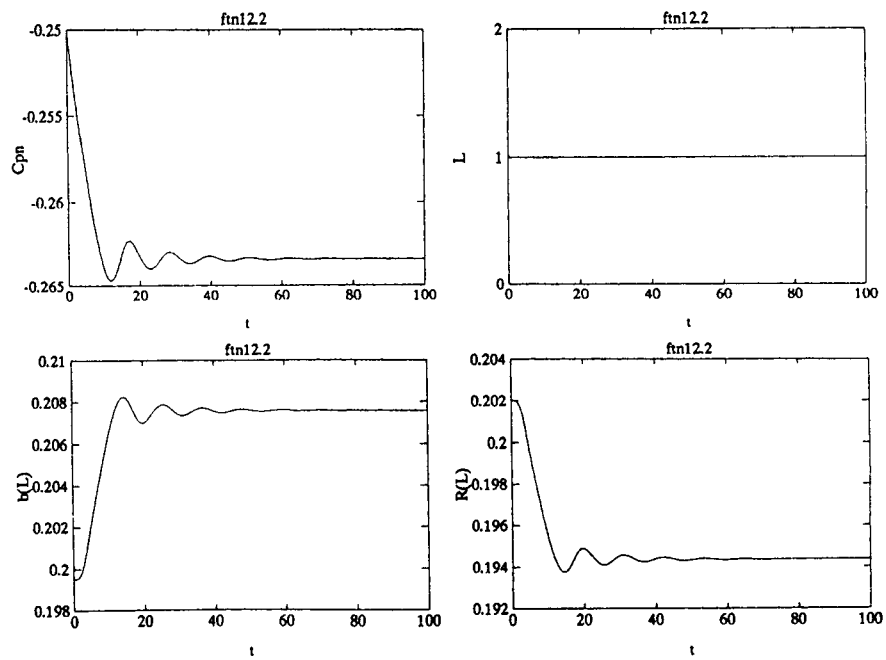

Figure 5. Pressure coefficient, convergence length and annular jet thickness and mean radius at the convergence point as functions of time for γ=4

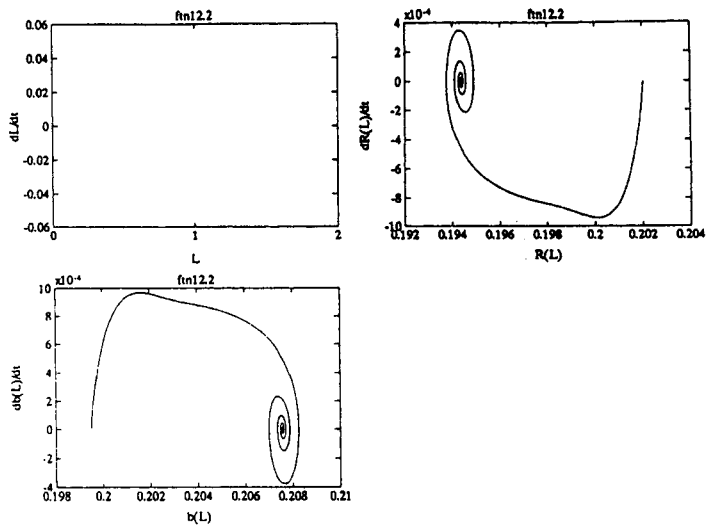

Figure 6. Phase diagrams for γ=4

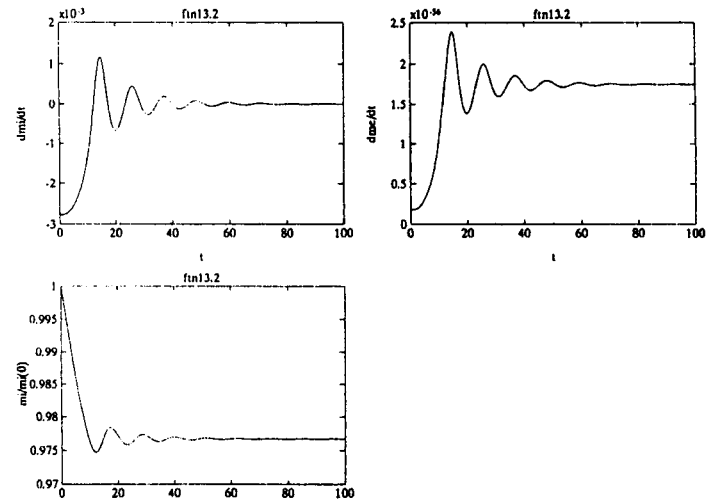

Figure 7. Mass transfer rates at the inner and outer interfaces and mass of the gases enclosed by the annular jet as functions of time for γ=4

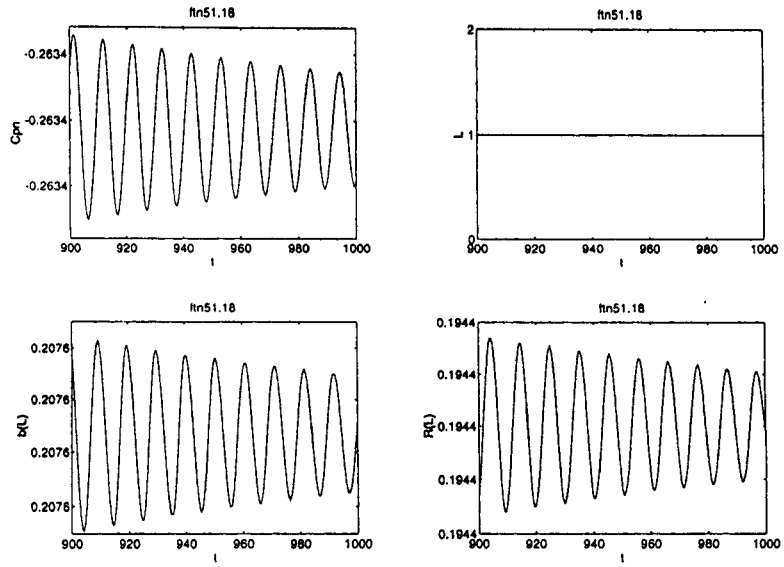

Figure 8. Pressure coefficient, convergence length and annular jet thickness and mean radius at the convergence point as functions of time for γ=4·8

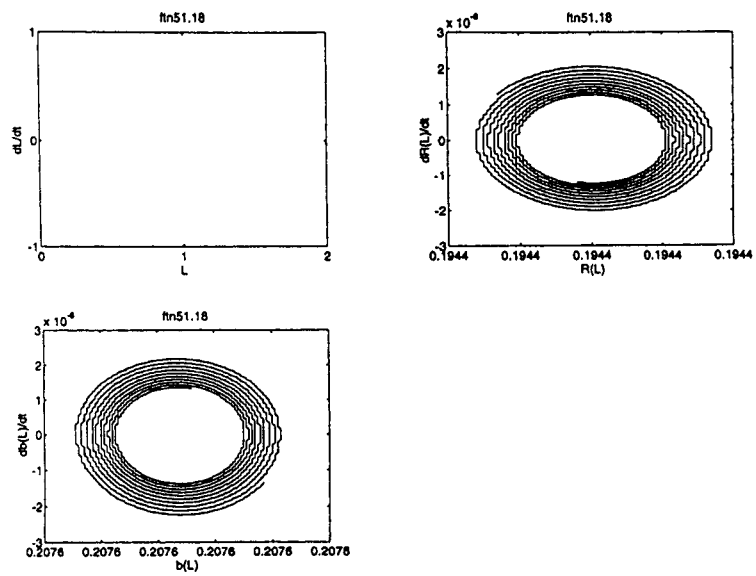

Figure 9. Phase diagrams for γ=4·8

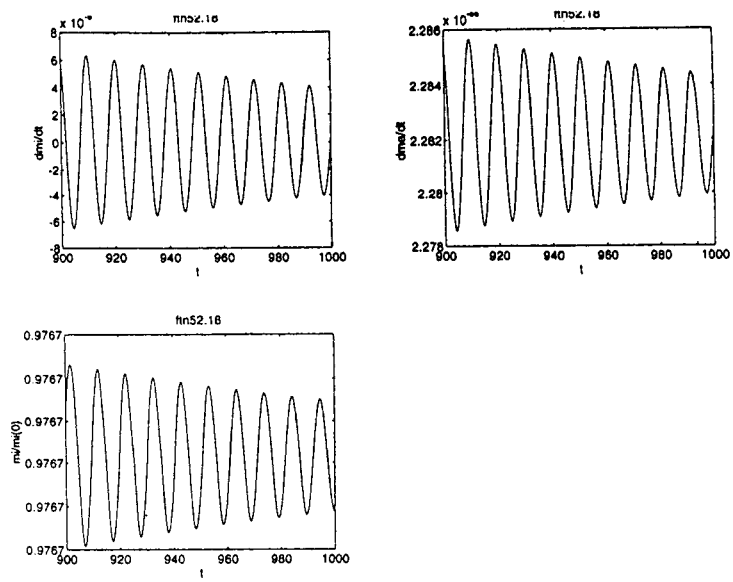

Figure 10. Mass transfer rates at the inner and outer interfaces and mass of the gases enclosed by the annular jet as functions of time for γ =4·8

thickness and mean radius at the convergence point are small. As a consequence, the mass transfer rates at the inner and outer interfaces are small and oscillate almost sinusoidally as functions of time (see Figure 13). The amplitudes of the oscillations of the thickness and mean radius at the convergence point are approximately equal to 0·00020 and 0·00015 respectively, whereas the amplitude of the oscillations in the mass transfer rate at the jet's inner interface is about 0·00035.

The results presented in Figures 8–10 and 11–13 indicate that a supercritical Hopf bifurcation occurs

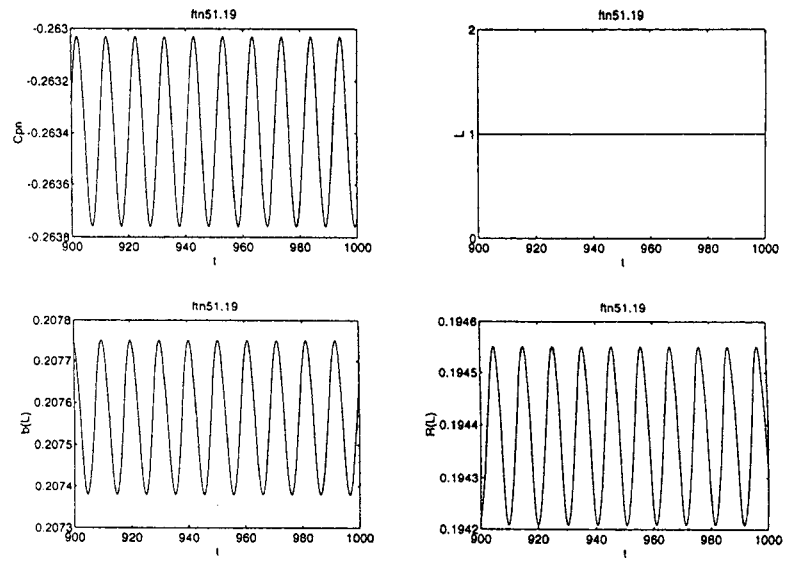

Figure 11. Pressure coefficient, convergence length and annular jet thickness and mean radius at the convergence point as functions of time for γ=4·9

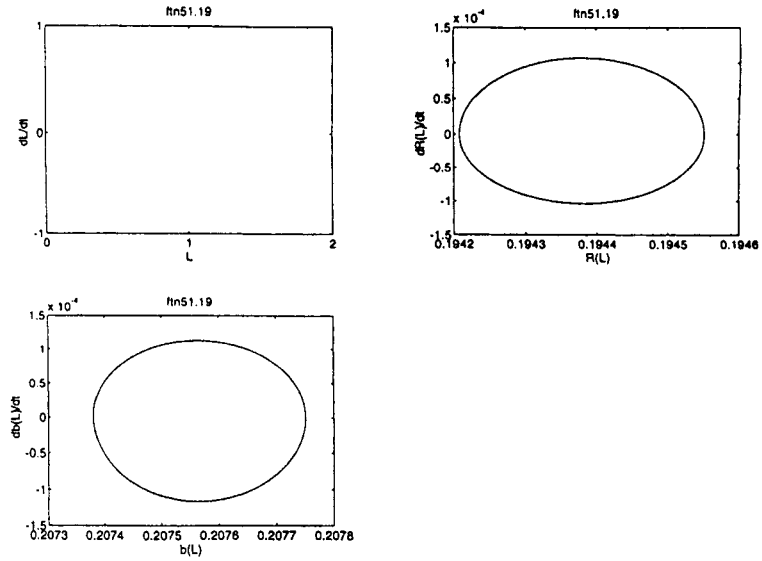

Figure 12. Phase diagrams for γ=4·9

for a value of γ between 4·8 and 4·9. In the next paragraphs we will examine the dynamic behaviour of the annular liquid jet beyond the Hopf bifurcation point, i.e. for values of γ larger than 4·9.

Figures 14–16 correspond to γ = 6 and indicate that both the shape and amplitude of the pressure coefficient oscillations are quite different from those observed for γ = 4·9. In particular, there has been a steepening in the rising part of the pressure coefficient and an increase in its amplitude. A similar

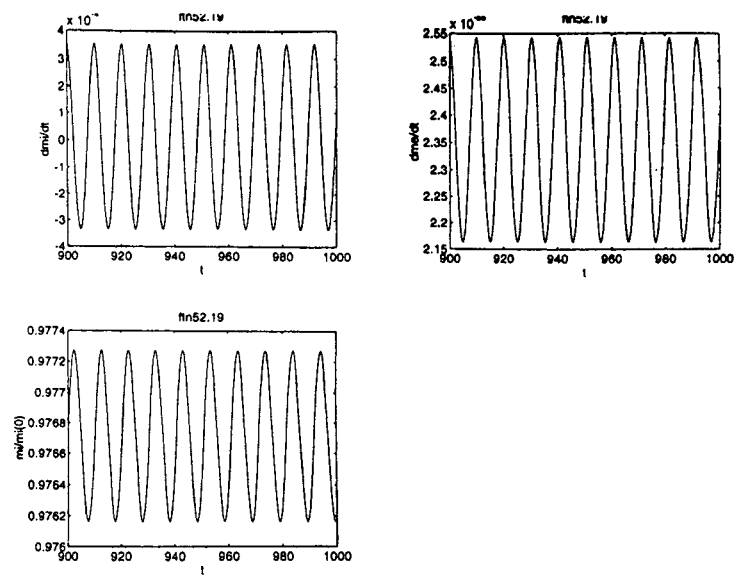

Figure 13. Mass transfer rates at the inner and outer interfaces and mass of the gases enclosed by the annular jet as functions of time for γ=4·9

behaviour can be seen in the jet mean radius at the convergence point, whereas the thickness at the convergence point has become steeper on its downward side. The amplitudes of the oscillations of the pressure coefficient and thickness and mean radius at the convergence point are 0·08, 0·003 and 0·0003 respectively. Comparisons between Figures 11 and 14 indicate that also the frequency of the oscillations decrease as γ is increased.

The changes in both the amplitude and frequency of the pressure coefficient oscillations as γ is increased can also be seen in Figures 17–19, which correspond to $\gamma = 10$. These figures indicate the steepening in the rising part of the pressure coefficient and deformations in the phase diagrams as γ is increased.

The effects of the Hopf bifurcation on mass transfer can be seen in Figures 12, 15 and 18, which indicate that the mass transfer rates increase as γ is increased. In particular, for a value of $\gamma = 10$, the mass transfer rate at the inner interface is a periodic function of time, is negative for most of the period of oscillation and exhibits a narrow spike where it is positive. Similar trends can be observed in the mass transfer rate at the outer interface. However, the most important consequence of the Hopf bifurcation can be seen for $\gamma = 10$. As shown in Figure 19, the mass of the gases enclosed by the annular liquid jet averaged over a period of oscillation is greater than unity, i.e. it is greater than the steady state initial value. This implies that the Hopf bifurcation has resulted in mass rectification under isothermal conditions. Note that the largest and smallest values of m_i are approximately 128% and 97% of $m_i(0)$ respectively, whereas the asymptotic, steady state value of m_i for $\gamma = 2$ was about 97·56% of $m_i(0)$.

The results presented in Figure 17 indicate that the pressure coefficient averaged over a period of oscillation is negative, i.e. the average pressure of the gases enclosed by the annular jet is smaller than that of the gases surrounding the jet. Figure 17 also indicates that the convergence length normalized by its initial value is constant. This result is consistent with the analytical and numerical studies of steady state, annular liquid jets reported in References 4 and 5.

Although not shown here, the oscillations in the volume enclosed by the annular jet have an amplitude of about 4% of the initial volume for $\gamma = 10$. Therefore, since the convergence length is

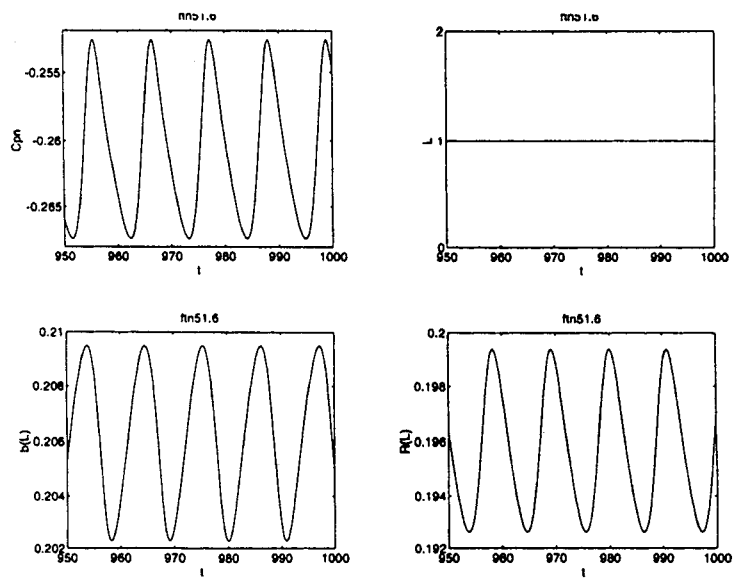

Figure 14. Pressure coefficient, convergence length and annular jet thickness and mean radius at the convergence point as functions of time for γ=6

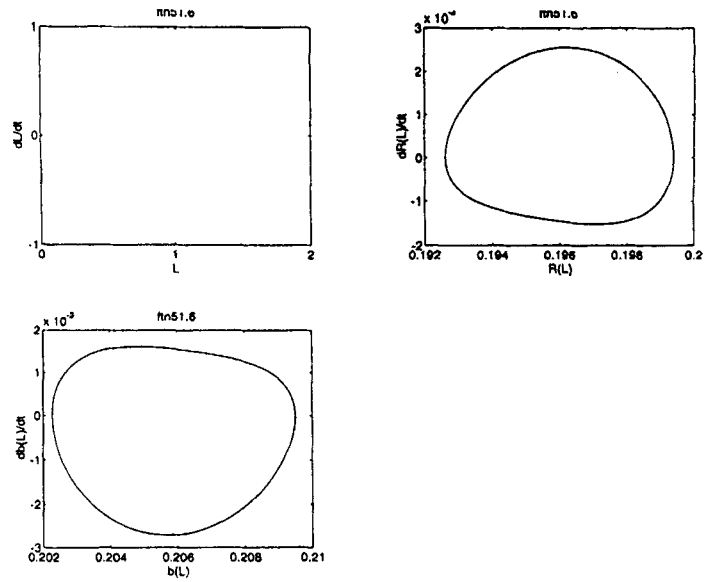

Figure 15. Phase diagrams for γ=6

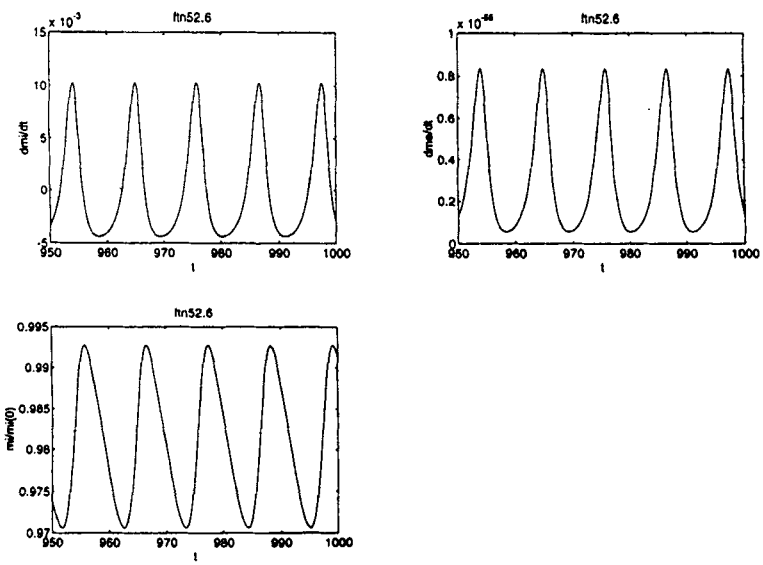

Figure 16. Mass transfer rates at the inner and outer interfaces and mass of the gases enclosed by the annular jet as functions of time for γ=6

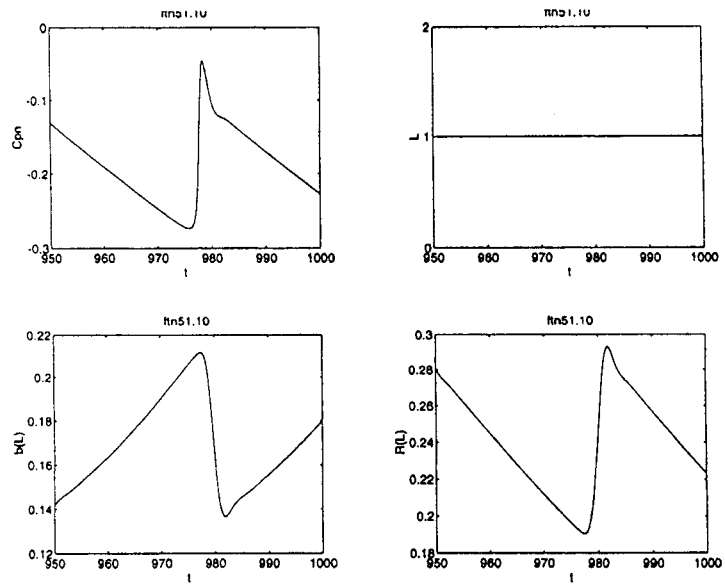

Figure 17. Pressure coefficient, convergence length and annular jet thickness and mean radius at the convergence point as functions of time for γ=10

independent of time, the oscillations in the volume enclosed by the jet's inner interface are due to the oscillations in the jet mean radius and thickness as indicated in Figure 17.

Calculations for γ=25 were also attempted, but no numerical convergence was achieved even for time steps smaller than 10^{-6}. This lack of convergence was attributed to the increase in amplitude of the pressure coefficient as γ is increased as discussed in previous paragraphs. As indicated in the analytical and numerical studies of References 4 and 5, under steady state operating conditions and for

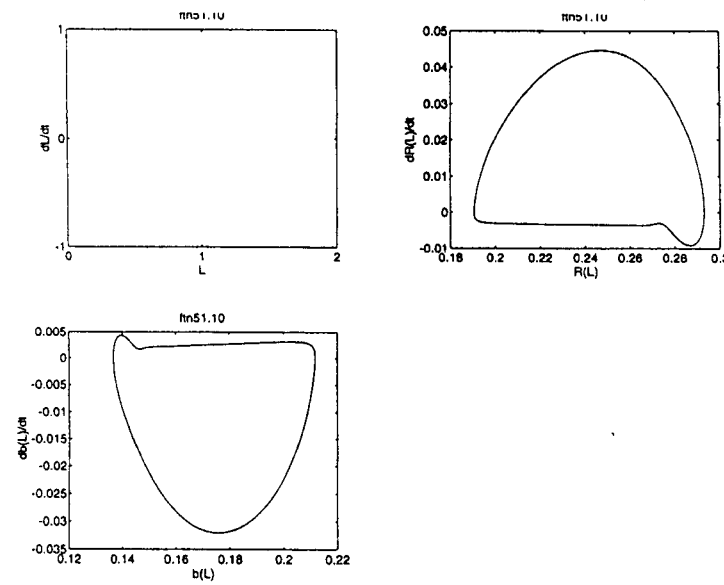

Figure 18. Phase diagrams for γ=10

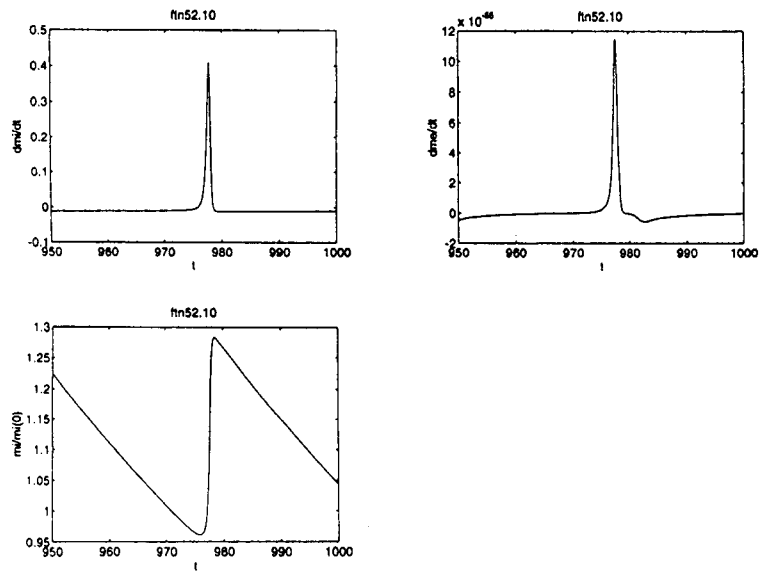

Figure 19. Mass transfer rates at the inner and outer interfaces and mass of the gases enclosed by the annular jet as functions of time for γ=10

long annular liquid jets and a nozzle exit angle of 0°, a pressure coefficient equal to unity results in a cylindrical annular jet, i.e. no enclosed volume is formed. It is possible that for large values of γ the pressure coefficient may exceed its steady state, critical value and no enclosed volume may result.

5. CONCLUSIONS

A numerical study of mass absorption by inviscid, thin, incompressible, underpressurized, annular liquid jets has been presented. The study is based on the assumptions that the gas–liquid interfaces are clean, the mass transfer resistances are negligible and the Mach number is small and has been performed as a function of the ratio of solubilities at the inner and outer interfaces of the annular liquid jet. It has been shown that, once the combustion of toxic wastes within the volume enclosed by the jet is extinguished, the dynamics of annular liquid jets with mass transfer depends on the solubility ratio. For solubility ratios less than a critical value located between 4·8 and 4·9, the annular liquid jet tends either monotonically or oscillatorily to a steady state at which the gas concentrations at the inner and outer interfaces are identically equal to zero. At the critical value there is a Hopf bifurcation characterized by periodic pressure coefficients and mass transfer rates. The amplitude and frequency of this periodic phenomenon increases and decreases respectively as the solubility ratio is increased. For a solubility ratio equal to 10, substantial mass rectification or enhancement has been observed as a consequence of the increase in the mass transfer rate during the compression of the gases enclosed by the jet. It has also been shown that the accurate determination of the dynamics of and mass transfer by annular liquid jets near to and beyond the Hopf bifurcation point is extremely sensitive to the time step, number of grid points and convergence criteria used to ensure convergence within the time step. If either the time step or the grid spacing is not sufficiently small, the mass transfer rate through the jet's inner interface cannot be determined accurately. As a consequence, the fluid dynamics of the liquid and the steep pressure coefficients and mass transfer spikes cannot be accurately resolved.

ACKNOWLEDGEMENTS

The research reported in this paper was supported by Project PB/91-0767 from the DGICYT of Spain.

REFERENCES

1. R. M. Roidt and Z. M. Shapiro, 'Liquid curtain reactor', *Report 85M981*. Westinghouse R&D Center, Pittsburgh, PA, 1985.
2. E. L. Cussler, *Diffusion: Mass Transfer in Fluid Systems*, Cambridge University Press, New York, 1984, pp. 242–245.
3. R. B. Bird, W. E. Stewart and E. N. Lightfoot, *Transport Pheonomena*, Wiley, New York, 1960, pp. 652–656.
4. J. I. Ramos, 'Liquid curtains—I. Fluid mechanics, *Chem. Eng. Sci.*, **43**, 3171–3184 (1989).
5. J. I. Ramos, 'Annular liquid jets: Formulation and steady state analysis, *Z. Angew. Math. Mech. (ZAMM)*, **72**, 565–589 (1992).
6. J. I. Ramos and R. Pitchumani, 'An analysis of boundary layers on liquid curtains', *J. Appl. Math. Phys. (ZAMP)*, **40**, 721–739 (1989).
7. M. H. I. Baird and J. F. Davidson, 'Annular jets—II. Gas absorption, *Chem. Eng. Sci.*, **17**, 473–480 (1962).
8. J. I. Ramos and R. Pitchumani, 'Liquid curtains—II. Gas absorption', *Chem. Eng. Sci.*, **45**, 1595–1604 (1990).
9. J. I. Ramos, 'Mass absorption by annular liquid jets: I. Analytical and numerical studies using the von Mises transformation', *Int. J. Numer. Methods Heat Fluid Flow*, **1**, 99–120 (1991).
10. J. I. Ramos, 'Mass absorption by annular liquid jets: II. Analytical and numerical studies using a linear mapping', *Int. J. Numer. Methods Heat Fluid Flow*, **1**, 121–141 (1991).
11. J. I. Ramos, 'Mass absorption by annular liquid jets: III. Numerical studies of jet collapse', *Int. J. Numer. Methods Heat Fluid Flow*, **2**, 21–36 (1992).
12. J. I. Ramos, 'Domain-adaptive finite difference methods for collapsing annular liquid jets', *Comput. Mech.: Int. J.*, **11**, 28–64 (1993).